Activation and dissociation of CO2 on the (001), (011), and (111) surfaces of mackinawite (FeS): A dispersion-corrected DFT study

N. Y. Dzade, A. Roldan, and N. H. de Leeuw

Articles you may be interested in

Activation and dissociation of CO₂ on the (001), (011), and (111) surfaces of mackinawite (FeS): A dispersion-corrected DFT study

N. Y. Dzade,[1,a)] A. Roldan,[2] and N. H. de Leeuw[1,2,a)]

[1]*Department of Earth Sciences, Utrecht University, Princetonplein 9, 3584 CC Utrecht, The Netherlands*
[2]*School of Chemistry, Cardiff University, Cardiff CF10 1DF, United Kingdom*

Iron sulfide minerals, including mackinawite (FeS), are relevant in origin of life theories, due to their potential catalytic activity towards the reduction and conversion of carbon dioxide (CO_2) to organic molecules, which may be applicable to the production of liquid fuels and commodity chemicals. However, the fundamental understanding of CO_2 adsorption, activation, and dissociation on FeS surfaces remains incomplete. Here, we have used density functional theory calculations, corrected for long-range dispersion interactions (DFT-D2), to explore various adsorption sites and configurations for CO_2 on the low-index mackinawite (001), (110), and (111) surfaces. We found that the CO_2 molecule physisorbs weakly on the energetically most stable (001) surface but adsorbs relatively strongly on the (011) and (111) FeS surfaces, preferentially at Fe sites. The adsorption of the CO_2 on the (011) and (111) surfaces is shown to be characterized by significant charge transfer from surface Fe species to the CO_2 molecule, which causes a large structural transformation in the molecule (i.e., forming a negatively charged bent $CO_2^{-\delta}$ species, with weaker C—O confirmed via vibrational frequency analyses). We have also analyzed the pathways for CO_2 reduction to CO and O on the mackinawite (011) and (111) surfaces. CO_2 dissociation is calculated to be slightly endothermic relative to the associatively adsorbed states, with relatively large activation energy barriers of 1.25 eV and 0.72 eV on the (011) and (111) surfaces, respectively. © *2015 AIP Publishing LLC.* [http://dx.doi.org/10.1063/1.4929470]

I. INTRODUCTION

The synthesis of liquid fuels and commodity chemicals from carbon dioxide (CO_2) is a promising alternative to conventional fossil fuels.[1,2] For this reason, considerable academic and industrial efforts have been dedicated to explore efficient means of reducing CO_2 and converting it into organic molecules, as precursors to fuels and chemicals feedstocks.[2–7] CO_2 utilization can help alleviate the environmental impact of greenhouse gas emissions, and it complements current technologies for carbon capture, sequestration, and storage.[1,2] The first step in CO_2 reduction on heterogeneous catalyst surfaces is the activation of the C=O bond and charge transfer for the eventual formation of an anion radical species.[2] A significant number of studies exist in the literature regarding the adsorption, activation, and conversion of CO_2 using both heterogeneous, e.g., on metal/metal oxide surfaces[8–11] or metal-organic frameworks,[12–15] and homogeneous reactions, e.g., transition metal complexes.[16–21]

More recently, transition metal sulfides have attracted significant attention for catalytic applications owing to their low cost, natural abundance, and prominent catalytic features. MoS_2 for instance has been widely used as an efficient catalyst for water splitting[22,23] and hydrodesulphurization,[24,25] whereas a recent report has shown its superior CO_2 reduction performance in an ionic liquid, compared to the noble metals, with a

high current density and low overpotential (54 mV).[26] Iron-nickel sulfide membranes formed in hydrothermal systems in the deep ocean floor are increasingly considered to be the early catalysts for a series of biochemical reactions leading to the emergence of life.[27–30] The anaerobic production of acetate, formaldehyde, and amino acids, and the nucleic acid bases (the organic precursors for larger biomolecules) are thought to have been catalyzed by small cubane (Fe, Ni)S clusters (for example, Fe_5NiS_8), which are structurally similar to the surfaces of present day sulfide minerals such as greigite (Fe_3S_4),[31] violarite ($FeNi_2S_4$),[32] and mackinawite (FeS).[33,34] In nature, the enzyme, carbon monoxide dehydrogenase (CODH), which has its primary active site as (Fe, Ni)S clusters, has been shown to efficiently and reversibly catalyze the reduction of CO_2 to CO.[35,36] Huber and Wächtershäuser demonstrated that it is possible to synthesize acetic acid on sulfide surfaces in conditions simulating Earth before life,[37] whereas a recent study has shown that Fe_3S_4 acts like a catalyst in the electro-reduction of CO_2 to methanol, and formic, acetic, and pyruvic acids under moderate conditions of pressure and temperature.[31]

In this study, we report the reactivity of the iron sulfide FeS towards the adsorption, activation, and reduction of CO_2 using first-principles density functional theory (DFT) calculations. FeS is a layered iron sulfide mineral that crystallises in the tetragonal structure, and it is considered to be the first iron sulfide phase formed from the reaction of Fe and S in low temperature aqueous environments.[38] Our study provides

---

a)Electronic addresses: N.Y.Dzade@uu.nl and N.H.Deleeuw@uu.nl

a mechanistic understanding of CO_2 activation and reduction on low-index mackinawite surfaces. First, we quantify the adsorption of CO_2 on the mackinawite (001), (011), and (111) surfaces and evaluate the electronic properties, including charge transfer. Second, we analyze the reaction pathways for CO_2 dissociation to CO and O, identifying the transition states (TS's) of the dissociation and calculating the activation energy barriers. Our results provide detailed theoretical evidence that FeS surfaces can activate the CO_2 molecule, and that subsequent dissociation of the molecule ($CO_2 \rightarrow CO + O$) occurs preferentially at Fe sites via significant charge transfer from these surface species.

II. COMPUTATIONAL DETAILS

The structures and total energies were determined using plane-wave density functional theory (PW-DFT) calculations within the Vienna *Ab-initio* Simulation Package (VASP code).[39–42] Long-range dispersion forces were accounted for in our calculations using the density functional theory with a correction for the long-range interactions (DFT-D2) method of Grimme,[43] which is essential for the accurate description of the FeS interlayer interactions, as well as the interactions between CO_2 and FeS surfaces.[33,34] The generalized gradient approximation (GGA), with the PW91 functional was used to calculate the total energies.[44,45] The interactions between the valence electrons and the cores were described with the projected augmented wave (PAW) method[46] in the implementation of Kresse and Joubert.[47] An energy cutoff of 400 eV for the plane-wave basis set was tested to be sufficient to converge the total energy of mackinawite and the Brillouin zone was sampled using a $11 \times 11 \times 7$ and $5 \times 5 \times 1$ Monkhorst-Pack[48] k-points mesh for bulk and surface calculations, respectively. Structural optimizations were performed using a conjugate gradients technique with an iterative relaxation of the atomic positions until the residual forces acting on the atoms reached 0.01 eV/Å.

The bulk mackinawite was modelled in the tetragonal structure (Figure 1(a)), for simplicity considering only the non-magnetic state which provides, in addition, best agreement of the lattice parameters with the experimental data.[49–51] Moreover, both room temperature neutron diffraction[52] and Mössbauer data[53] at 4.2 K with an external field testify to the absence of an iron magnetic moment in mackinawite. In

earlier studies, we have demonstrated that the inclusion of dispersion corrections yields improved agreement between the predicted lattice parameters ($a = 3.587$ Å, $c = 4.908$ Å, and $c/a = 1.368$)[33,34] and those measured experimentally.[49–51] The calculated electronic density of states (DOS) (Figure 1(b)) shows metallic character, with the electronic states of the Fe d-orbitals dominating the regions around the Fermi level, in agreement with the metallic nature deduced by Vaughan and Ridout.[53] These features are consistent with earlier DFT results of mackinawite.[54–56]

The (001), (011), and (111) surfaces, which are the dominant growth surface FeS,[34,57] were created from the relaxed bulk material using the METADISE code,[58] which not only considers periodicity in the plane direction but also provides the different atomic layer stacking resulting in a zero dipole moment perpendicular to the surface plane, as is required for reliable and realistic surface calculations.[59] Different slab and vacuum thicknesses as well as numbers of relaxed layers were tested for the different surfaces until convergence within 1 meV per cell was achieved. The converged slab thicknesses used to model the (001), (011), and (111) surfaces were constructed of 6, 9, and 12 atomic layers, respectively, and in every simulation cell, a vacuum region of 15 Å perpendicular to the surface was tested to be sufficient to avoid interactions between periodic slabs.

Schematic illustrations of the relaxed structures of the FeS (001), (011), and (111) surfaces are displayed in Figure 2. The (001) surface, with a relaxed surface energy of 0.19 J m^{-2},[34] is by far the most stable surface of FeS, because its creation only involves breaking the weak van der Waals interactions between the FeS layers which results in negligible relaxation of the surface species. These results are in excellent agreement with the results of Ohfuji and Rickard using selected area electron diffraction (SAED) analyses on FeS nanocrystals.[57] We have calculated the surface energies by considering both the Fe- and S-terminated surfaces of the (011) and (111) index surfaces but found that the S-terminated (011) surface has a much higher surface energy (1.47 J m^{-2}) than the Fe-terminated surface (0.95 J m^{-2}), whereas for the (111) surface, the Fe-termination was calculated to have a higher surface energy (1.69 J m^{-2}) than the S-termination (1.51 J m^{-2}). In the remainder of this work, we have therefore focussed on the Fe-terminated (011) surface and the S-terminated (111) surface, in our calculations of their affinity towards CO_2 as only the most stable terminations will primarily be present in FeS crystals.
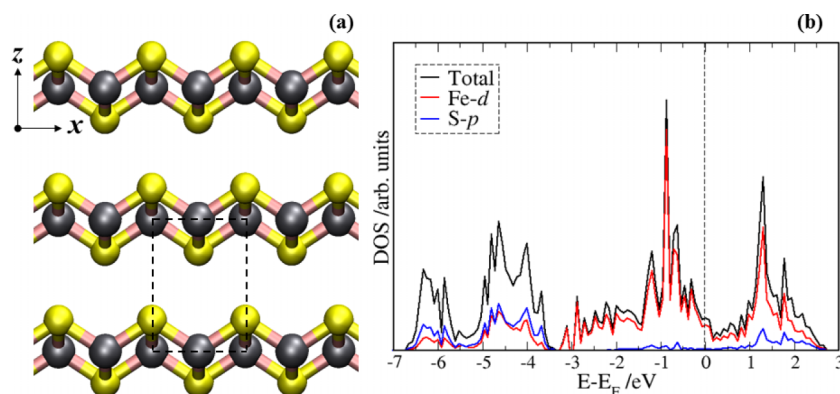

FIG. 1. The layered structure of bulk mackinawite (a) with the tetragonal unit cell highlighted by dashed lines, (b) the electronic density of states, showing the total and projections on the Fe d-states and S p-states. (Colour scheme: Fe = grey and S = yellow.)
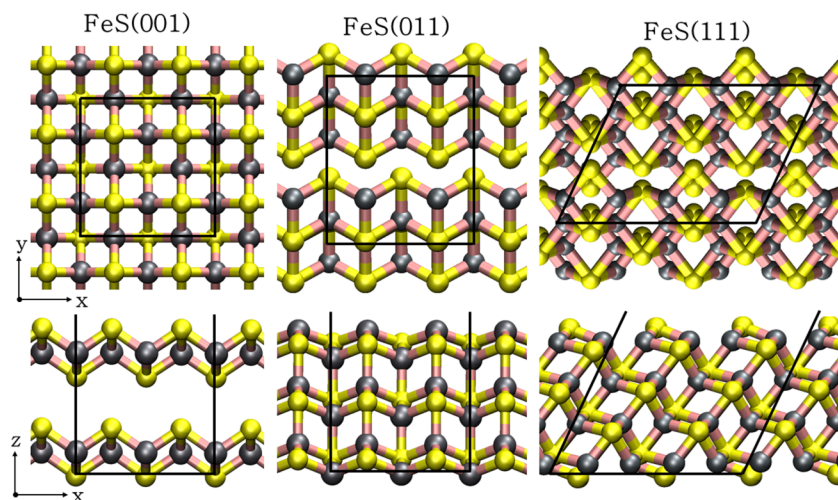
FIG. 2. Schematic illustration of the top (top row) and side (bottom row) views of the relaxed structures of the (001), (011), and (111) surfaces of FeS. A (2×2) unit cell size is highlighted by dashed lines. (Colour scheme: Fe = grey and S = yellow.)

In modeling the interaction of the CO_2 adsorbate with the FeS surface slabs, the atoms of the adsorbate and the three topmost layers of the slab were allowed to relax unconstrainedly until residual forces on all atoms reached 0.01 eV/Å. Symmetry constraints were not included in the structural optimization; in particular, the CO_2 molecule was free to move away laterally and vertically from the initial site or to reorient itself to find the minimum energy adsorption structure. The energy of adsorption for carbon dioxide on the FeS surfaces is calculated using the relation

$$E_{ads} = E_{surf+CO_2} - (E_{surf} + E_{CO_2}), \qquad (1)$$

where E_{surf} is the total energy of the FeS surface slab, E_{CO_2} is the total energy of the CO_2 molecule (optimized in a cubic unit cell of size 20 Å), and $E_{surf+CO_2}$ is the total energy of the composite system. By this definition, a negative value of E_{ads} corresponds to an exothermic and thus thermodynamically favourable adsorption process. A Bader analysis was carried out for all the CO_2—FeS systems, using the code developed by Henkelman and co-workers[60,61] in order to quantify the charge transfer between the surfaces and CO_2 moiety. The climbing image nudged elastic band (CI-NEB) method was used to locate the transition state and reaction activation energy bar-

riers of the CO_2 dissociation process.[62,63] Identified transition states were further confirmed through frequency calculations, in which only one imaginary frequency is obtained corresponding to the reaction coordinate. The activation energy barrier (E_a) is defined as the total energy differences between the initial state (IS) and the saddle point, and the reaction energies (ΔE) are calculated as the total energy difference between the final state (FS) and the initial state.

III. RESULTS AND DISCUSSIONS

A. CO_2 adsorption on FeS(001)

The first set of CO_2 adsorption calculations were performed on the most stable (001) surface, where we found very weak interaction between the surface and adsorbate. The CO_2 molecule was introduced onto the surface in horizontal and vertical orientations, but during energy minimization, it moved away perpendicularly from the surface whilst remaining in a linear conformation. The optimized CO_2 adsorption geometries on the (001) surface are displayed in Figure 3, with the adsorption energies and structural parameters summarized in Table I. The optimized parallel CO_2 configuration (denoted L(I)-horizontal) released an adsorption energy of 0.20 eV,
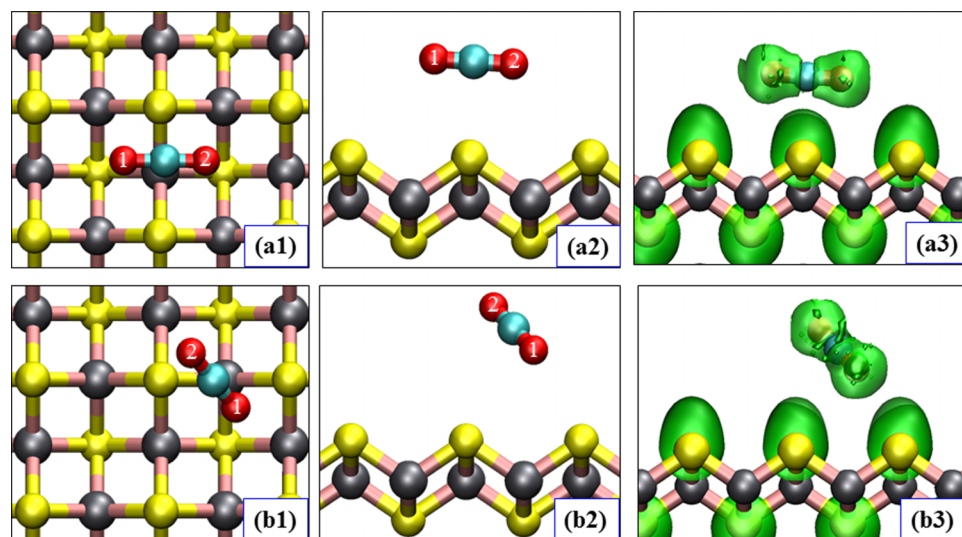

FIG. 3. Top (left) and side (middle) views of the optimized horizontal (top row) and oblique (bottom row) adsorption configurations of CO_2 on the FeS(001) surface. The surfaces and contours of the electron localization function are shown on the right panels. (Colour scheme: Fe = grey, S = yellow, O = red, and C = cyan.)

TABLE I. Adsorption energies, representative geometrical parameters, vibrational frequencies, and variation of the total Bader charge of a CO_2 molecule adsorbed at the (001), (011), and (111) surfaces of FeS. In the notation η^x(m, n), x denotes the number surface Fe sites the CO_2 interacts with, and the letters in brackets, m and n denote the interacting atoms.

Surface	Bonding type	E_{ads}/eV	d(C—O$_1$)/Å	d(C—O$_2$)/Å	d(C—Fe)/Å	d(O$_1$—Fe)/Å	d(O$_2$—Fe)/Å	α(OCO)/°	ν_{as}/cm^{-1}	ν_s/cm^{-1}	ν_b/cm^{-1}	Δq(CO$_2$)/e$^-$
	CO_2 (gas phase)	...	1.176	1.176	...	...	...	180.0	2373	1323	631	0.00
(001)	L1–oblique	−0.16	1.178	1.176	4.666	4.083	...	179.8	2357	1317	593	0.00
	L2–horizontal	−0.20	1.176	1.176	4.013	4.222	4.149	179.6	2349	1319	628	0.00
(011)	L1–oblique	−0.25	1.177	1.177	3.092	2.520	3.045	179.2	2340	1302	615	−0.02
	B(I)–η^2(O,O)	−0.39	1.243	1.244	...	2.007	1.998	135.5	1683	1134	627	−0.33
	B(II)–η^1(C,O)	−0.45	1.253	1.202	2.015	2.073	...	146.1	1921	1140	599	−0.40
	B(III)–η^2(C,O)	−0.73	1.283	1.245	1.918	2.086	2.186	138.0	1703	1155	691	−0.69
(111)	L(I)–vertical	−0.28	1.185	1.168	...	2.314	...	179.5	2349	1323	611	−0.03
	L(II)–oblique	−0.35	1.183	1.166	...	2.231	...	178.3	2357	1314	584	−0.04
	B(I)–η^2(C,O)	−0.68	1.295	1.214	1.998	1.903	2.790	130.8	1712	1104	703	−0.63
	B(II)–η^2(C,O,O)	−0.87	1.242	1.241	2.105	2.112	2.111	138.7	1764	1173	654	−0.80

whereas the tilted configuration (denoted L(II)-oblique) released an adsorption energy of 0.16 eV. Consistent with this weak physisorption, no charge transfers were observed between the (001) surface and the CO_2 molecule upon adsorption and the C—O bond distances remained relatively unaffected. The weak interaction of the CO_2 molecule with the (001) surface can be attributed to the steric repulsion between the oxygen atoms and the S atoms terminating the (001) surface, as shown by the electron localization function displayed in Figure 3.

B. CO_2 adsorption on FeS(011)

In contrast to the (001) surface, the CO_2 molecule interacts strongly with the (011) surface in four different adsorption configurations, as displayed in Figure 4. The energies of adsorption, geometrical parameters, vibrational frequencies, and variations in the total charge of the adsorbed CO_2 molecule (Δq(CO_2)) are summarized in Table I. For the first configuration, the CO_2 molecule binds at a surface Fe site, tilted relative to the surface normal, and retaining a nearly linear structure (α(OCO) = 179.2° and d(C—O) = 1.177 Å). This binding mode is denoted as L(I) in Figure 4(a), and it has an adsorption energy of −0.25 eV. The remaining three adsorption structures identified on the (011) surface have bent CO_2 structures and are denoted as B(I), B(II), and B(III) in Figure 4. Among the bent CO_2 adsorption configurations, B(III) is found to be the energetically most favourable binding mode (Figure 4(d)), with an adsorption energy of −0.73 eV. In this bent configuration [α(OCO) = 138.0°], one O atom of the CO_2 molecule is bound to a surface Fe, and the C atom is bound to an adjacent Fe atom. The two C—O bonds in B(III) are elongated, calculated at 1.283 Å and 1.235 Å, respectively, compared to the gas phase C—O bond length of 1.176 Å, indicating that the C—O bonds are somewhat activated.

The other bent structures, B(I) and B(II), have adsorption energies of −0.39 eV and −0.45 eV, respectively. In B(I), the CO_2 molecule interacts with two surface Fe atoms via both oxygen atoms, whereas in B(II), the molecule binds via the C and one O atom at the same Fe site. Similar to the B(III) configuration, in both B(I) and B(II), the CO_2 molecule exhibits a bent configuration with the α(OCO) angle, respectively, calculated at 135.5° and 146.1°. The two C—O bonds in B(I) are elongated (both calculated at 1.244 Å) compared to the gas phase molecule at 1.176 Å. The surface-bound C—O bond in B(II) is calculated at 1.253 Å, whereas the non-interacting C—O bond is 1.202 Å. The stretched C—O bond lengths indicate weaker C—O bonds due to the π-antibonding occupation and activation of the molecule, which has implications for further chemical reactions on the surface, such as the reduction of the CO_2, molecule, discussed in Section III E.

C. CO_2 adsorption on FeS(111)

Four stable configurations were found on the (111) surface: two nearly linear (L(I) and L(2)) and two bent (B(I) and B(II)) adsorption configurations, as shown in Figure 5. Shown in Table I are the energies of adsorption, geometrical parameters, vibrational frequencies, and variations in the total
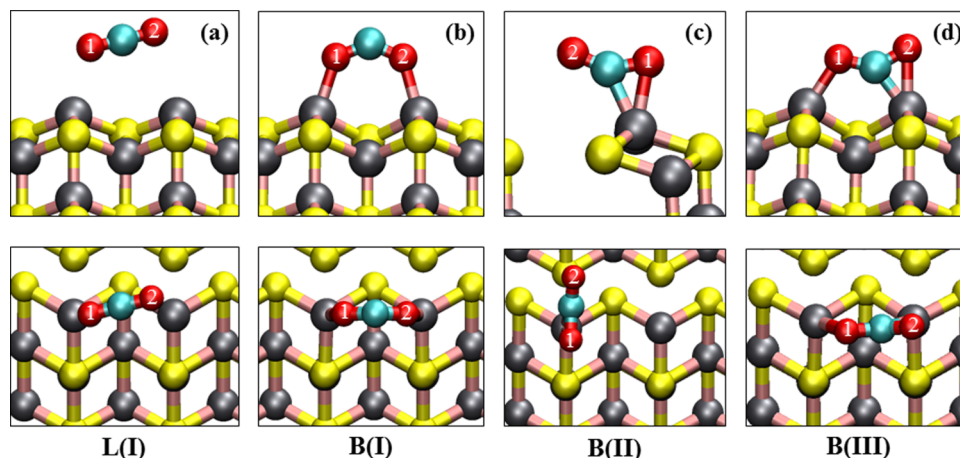
FIG. 4. Side (top) and top (bottom) views of the optimized adsorption configurations of CO_2 on FeS(011) surface. (Colour scheme: Fe = grey, S = yellow, O = red, and C = cyan.)
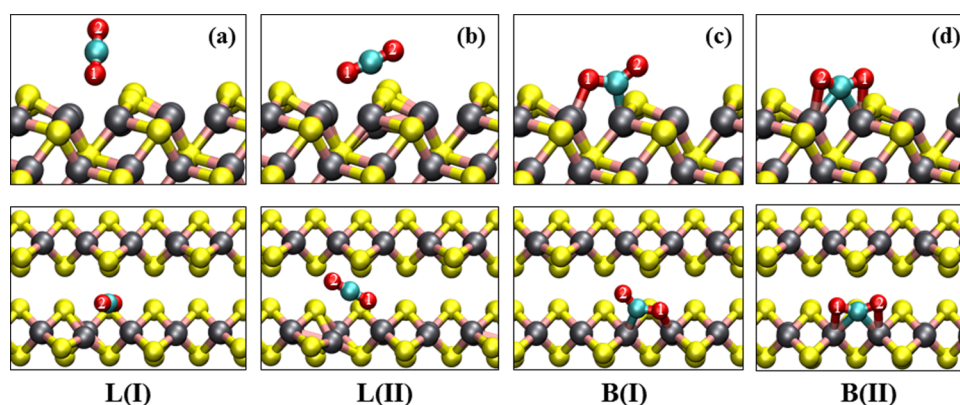

FIG. 5. Side (top) and top (bottom) views of the optimized adsorption configurations of CO_2 on FeS(111) surface. (Colour scheme: Fe = grey, S = yellow, O = red, and C = cyan.)
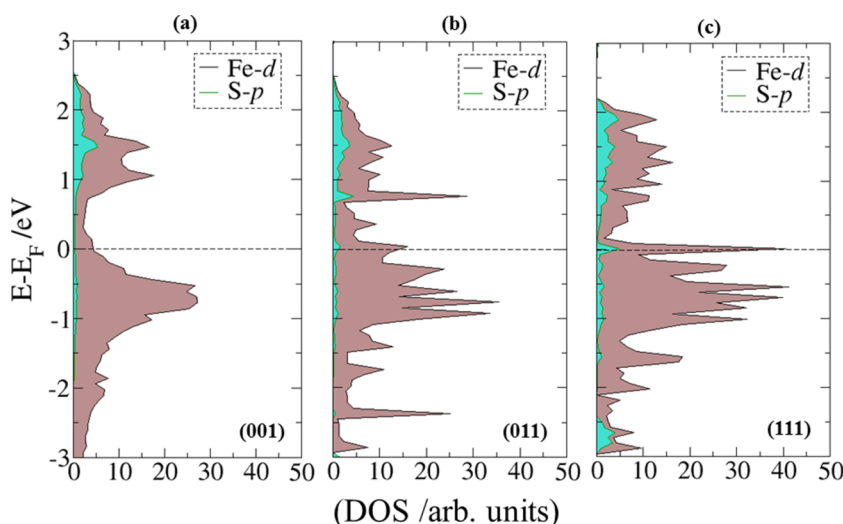

FIG. 6. Electronic density of states of (a) FeS(001), (b) FeS(011), and (c) FeS(111) naked surfaces projected on the Fe-d (violet region) and S-p (turquoise region) states. The dashed line corresponds to the Fermi level. Electron density of the Fe-d states at the Fermi level for the different surface increases in the order (001) < (011) < (111).

charge of the adsorbed CO_2 molecule. The strongest energy of adsorption (E_{ads} = −0.87 eV) is calculated for the B(II) configuration (Figure 5(d)), wherein the CO_2 molecule binds via all three atoms with the C atom bridging between two Fe atoms. The CO_2 molecule exhibits a bent configuration (α(OCO) = 138.7°), and the two C—O bonds in CO_2 are elon-

gated to 1.242 and 1.241 Å, compared to 1.176 Å in the gas phase. The next stable bent CO_2 configuration (B(I)), shown in Figure 5(c), has an adsorption energy of −0.68 eV, and the α(OCO) angle is 130.8°. The C—O bonds are elongated particularly the surface-bound one, (1.295 Å), compared to the gas phase CO_2 molecule. The two nearly linear CO_2 adsorption
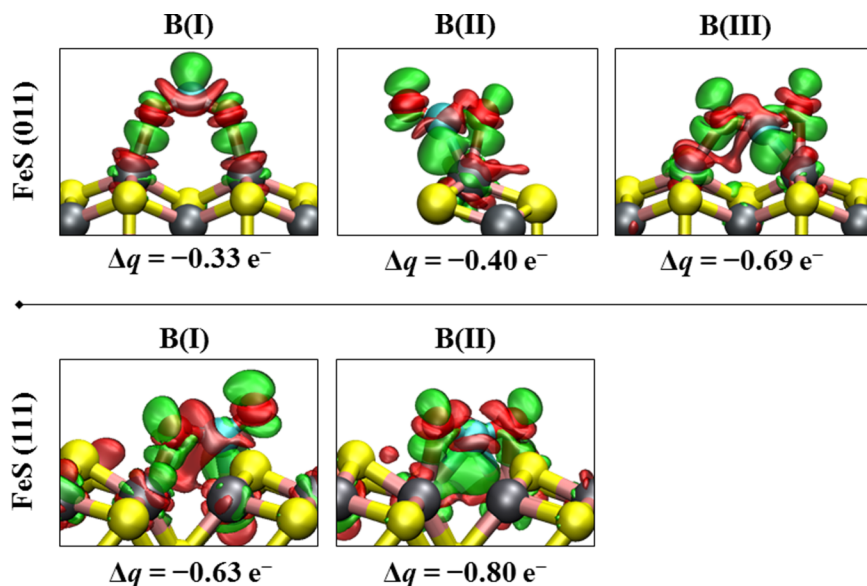
FIG. 7. Electron density difference plot of bent CO_2 adsorption structures on FeS(011), top row, and FeS(111), bottom row, showing charge transfer in the regions between the CO_2 and the surface Fe atoms upon adsorption. Green contours indicate electron density increase by 0.02 electrons/Å^3 and orange contours indicate electron density decrease by 0.02 electrons/Å^3.

complexes gave weak binding energies, with the L(I)-vertical and L(II)-oblique configurations releasing energies of 0.28 eV and 0.35 eV, respectively. The α(OCO) angles in the L(I) and L(II) configurations are, respectively, 179.5° and 178.3°, and in both cases, the C—O bond lengths are not affected significantly.

D. Electronic and vibrational analyses

As the CO_2 molecule may accept electrons into its lowest unoccupied molecular orbital to form negatively charged bent species ($CO_2^{-\delta}$), we have performed Bader charge analyses on the FeS—CO_2 adsorption systems in order to quantify the electron transfer from the surface to the CO_2 molecule. From the variation of the charges on the CO_2 molecule ($\Delta q(CO_2)$) in the various adsorption configurations (Table I), we observe clear charge transfer from the FeS surfaces to the adsorbed CO_2 molecule, which is especially prominent in the case of the B(II) $- \eta^2$(C, O, O) configuration on the (111) surface (Figure 5(d)), where a net charge of 0.80 e$^-$ is transferred to the adsorbed CO_2 molecule. In the most stable configuration on the (011) surface, B(III) $- \eta^2$(C, O) (Figure 4(d)), the CO_2 molecule gained a net charge of 0.69 e$^-$ from the surface species.

To clarify the source of the negative charge from the FeS (011) and (111) surfaces to the CO_2 molecule, we have calculated the electronic DOS, projected on the Fe-d and S-p states of the (001), (011), and (111) surfaces, as displayed in Figure 6. The density of states at the Fermi energy level (E$_F$) roughly determines the availability of electrons for a given reaction.[64] We found that the Fe d-states dominate the regions around the Fermi level in the electronic structure of the three low-index surfaces, indicating that the FeS catalytic activity should be primarily linked to the surface Fe d-states, whereas the S atoms provide negligible p-states at the Fermi level. The Fe d-states originating from the (111) surface are approximately twice as larger as those of the (011) surface at the Fermi level, which is reflected in more electron density being transferred from the (111) surface to the CO_2 upon adsorption, than on the (011). The (001) has the least number of Fe d-states available at the Fermi level and hence shows the weakest interaction with the CO_2 molecule.

Further insight into local charge rearrangement within the CO_2—FeS surface system can be gained from the electron density difference, obtained by subtracting from the charge density of the total adsorbate-substrate system, the sum of the charge densities of the CO_2 molecule and the clean FeS surface,

FIG. 8. Calculated reaction energy profile of CO_2 dissociation on the FeS (011) surface. The insets show the structures of the initial (IS), transition (TS), and final (FS) states. The asterisks (∗) denote the adsorbed species.
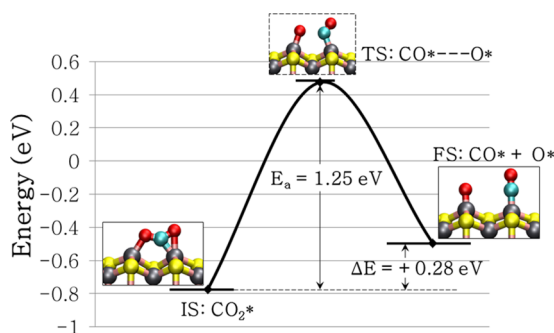

FIG. 9. Calculated reaction energy profile of CO_2 dissociation on the FeS (111) surface. The insets show the structures of the initial (IS), transition (TS), and final (FS) states. The asterisks (∗) denote the adsorbed species.
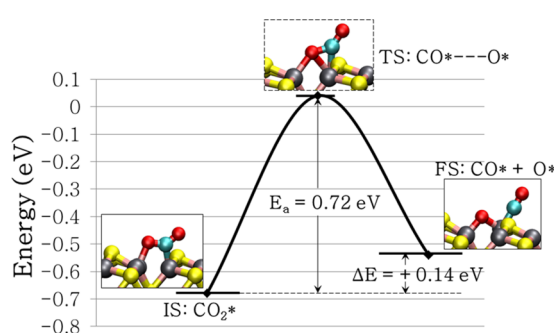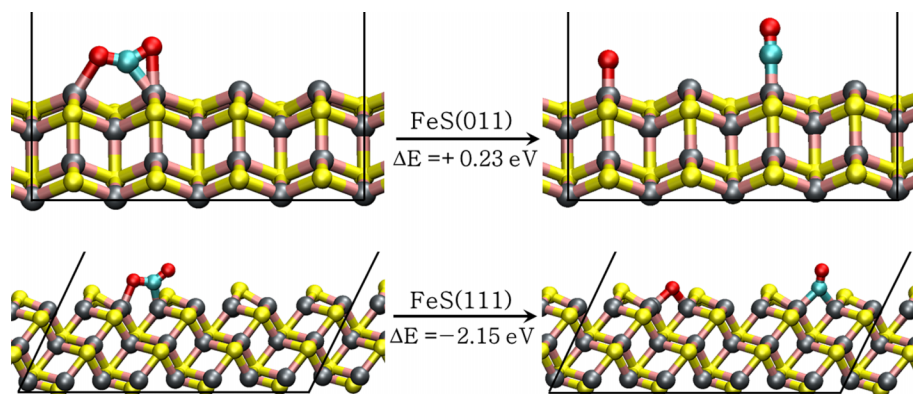
FIG. 10. FeS (011) and (111) surfaces with initial adsorbed CO_2 (left) and final CO and O states after diffusion to next nearest neighbour sites (right). (Colour scheme: Fe = grey, S = yellow, O = red, and C = cyan.)

calculated using the same geometry as the adsorbate-substrate system. Shown in Figure 7 are the electron density difference isosurface plots, revealing electron redistribution within the CO_2—FeS systems for the bent CO_2 configurations on the (011) and (111) surfaces. It can be seen from Figure 7 that the adsorbed CO_2 is activated, with a net negative charge localized on the oxygen atoms. Consistent with the large charge transfer to the CO_2 molecule upon adsorption, we observe significant structural transformation from linear to negatively charged $(CO_2^{\delta-})$ bent species, with elongated C—O bond distances (Table I). The stretched C—O bonds are confirmed by the calculated vibrational frequencies presented in Table I. For all the bent CO_2 configurations, we note a significant red-shift in the C—O symmetric (υ_s) and asymmetric (υ_{as}) stretching modes relative to the linear gas phase molecule, indicating that the CO_2 molecule is considerably activated. At the (001) surface, where no charge transfer was observed between the surface and the CO_2 molecule, the C—O stretch vibrational frequencies remain close to the gas-phase values of 2373 and 1323 cm^{-1}.

E. CO_2 dissociation on (011) and (111) surfaces

The results presented above show that CO_2 adsorbs strongly on the FeS (011) and (111) surfaces, where the adsorption process results in significant weakening of the C—O bonds of the carbon dioxide molecule. We now seek to determine how the differences in structure and electronic properties, of both the catalyst and the adsorbate, may dictate the reactivity of the system with respect to CO_2 dissociation to form surface-bound CO and O species. We have considered as starting structures, the B(III) configuration on the (011) surface and the B(I) configuration on the (111), because these adsorption structures exhibit the largest C—O bond lengthening. In both cases, the calculated reaction energies (ΔE) show that the dissociation reaction at the surfaces is slightly endothermic at +0.28 and +0.14 for the (011) and (111) surfaces, respectively. To determine the transition state and obtain an estimate of the energy barrier for the dissociation process, we have applied the CI-NEB methodology on a series of configurations connecting the two points of interest, the starting surface-bound CO_2 and the final adsorbed CO + O. The minimum energy pathways for CO_2 dissociation from these starting structures on the (011) and (111) surfaces are displayed in Figures 8 and 9, respectively.

The activation energy barrier (E_a) for the dissociation of CO_2 on the (011) and (111) surfaces are, respectively, calculated at 1.25 eV and 0.72 eV. The higher energy barrier for the dissociation of CO_2 on the (011) surface can be attributed to the additional energy required to pull the second oxygen (O2) from the surface Fe atom. On the (011) surface, the dissociated CO and O species bind atop to adjacent Fe atoms (the inset, FS, on Figure 8), whereas on the (111) surface, the dissociated O atom binds at a bridge site between two adjacent surface Fe atoms, whereas the CO moiety binds via the C atom atop a Fe site (the inset, FS, in Figure 9). Using a (4×2) unit cell, we also investigated the energy states of the dissociated species; when the CO and O fragments had diffused away from each other to second nearest neighbour adsorption sites, shown pictorially in Figure 10, we found that on the (011) surface, the final CO_2 dissociated states were still at a higher energy, by 0.23 eV, than the initial adsorbed CO_2 state. However, on the (111) surface, the overall dissociation process became highly exothermic, $\Delta E = -2.15$ eV, as the final states are lower in energy than the initial state with adsorbed CO_2. This suggests that the (111) surface favours the dissociation under low CO_2 pressure and when the dissociated species diffusion across the surface is much faster than the association process.

IV. SUMMARY AND CONCLUSIONS

We have performed analyses of the geometries, electronic and vibrational properties, and reaction energetics of carbon dioxide adsorption, activation, and dissociation on the mackinawite (001), (011), and (111) surfaces, using DFT-D2. We found that the structure of the surface plays an important role in the activation of CO_2 on mackinawite. The energetically most stable (001) surface shows the least reactivity towards CO_2 adsorption, whereas the (011) and (111) surfaces strongly adsorb the molecule, preferentially at Fe sites via charge transfer from these surface species as confirmed by Bader charge analysis. Elongation of the C—O bonds is observed in the adsorbed molecule on the (011) and (111) surfaces compared to the gas phase molecule, and the CO_2 molecule activation was confirmed via vibrational frequency analysis. From the calculated reaction energies and reaction barriers, we demonstrate that the (111) surface displays stronger reactivity towards CO_2 dissociation than the (011) surface. However, both reaction energy barriers and the catalytic dissociation processes are

energetically unfavourable, unless rapid diffusion of the CO and O dissociation products takes place, which would make the overall dissociation process on the (111) surface energetically favourable.

The calculated vibrational frequencies could be used to obtain the Gibbs free energies of the adsorption processes and to estimate TPD desorption temperatures, which can then be compared with future experiments in this area, which is the subject of future work. The current study, however, improves our understanding of how the different FeS surface structures dictate their reactivity toward CO_2 adsorption and dissociation, which and should assist experimentalists in the development of more efficient FeS catalysts with reactive surfaces. Future work will also include investigations of the same catalytic processes on defect or impurity-containing FeS surfaces to investigate their effect on the reaction kinetics and thermodynamics.

ACKNOWLEDGMENTS

[1]M. Aresta, *Carbon Dioxide as Chemical Feedstock* (Wiley-VCH, Weinheim, 2010).

[2]G. Centi and S. Perathoner, Top. Catal. **52**, 948 (2009).

[3]V. Havran, M. P. Duduković, and C. S. Lo, Ind. Eng. Chem. Res. **50**, 7089 (2011).

[4]A. J. Morris, G. J. Meyer, and E. Fujita, Acc. Chem. Res. **42**, 1983 (2009).

[5]S. C. Roy, O. K. Varghese, M. Paulose, and C. A. Grimes, ACS Nano **4**, 1259 (2010).

[6]R. D. Richardson, E. J. Holland, and B. K. Carpenter, Nat. Chem. **3**, 301 (2011).

[7]J. Baltrusaitis and V. H. Grassian, J. Phys. Chem. B **109**, 12227 (2005).

[8]P. Liu, Y. M. Choi, Y. Yang, and M. G. White, J. Phys. Chem. A **114**, 3888 (2010).

[9]E. A. Carter, Science **321**, 800 (2008).

[10]T. Yan, S. Wang, Y. Zhou, Z. Cao, and G. Li, J. Phys. Chem. C **113**, 19389 (2009).

[11]S. F. Li and Z. X. Guo, J. Phys. Chem. C **114**, 11456 (2010).

[12]D. Saha, Z. Bao, F. Jia, and S. Deng, Environ. Sci. Technol. **44**, 1820 (2010).

[13]B. Arstad, H. Fjellvåg, K. O. Kongshaug, O. Swang, and R. Blom, Adsorption **14**, 755 (2008).

[14]F. Salles, A. Ghoufi, G. Maurin, R. G. Bell, C. Mellot-Draznieks, and G. Férey, Angew. Chem., Int. Ed. **47**, 8487 (2008).

[15]L. Valenzano, B. Civalleri, S. Chavan, G. T. Palomino, C. O. Areán, and S. Bordiga, J. Phys. Chem. C **114**, 11185 (2010).

[16]D. Walther, M. Rubens, and S. Rau, Coord. Chem. Rev. **182**, 67 (1999).

[17]Y. Ohnishi, T. Matsunaga, Y. Nakao, H. Sato, and S. Sakaki, J. Am. Chem. Soc. **127**, 4021 (2005).

[18]D. Darensbourg, J. Chem. Rev. **107**, 2388 (2007).

[19]M. Isaacs, J. C. Canales, M. J. Aguirre, G. Estiu, F. Caruso, G. Ferraudi, and J. Costamagna, Inorg. Chim. Acta **339**, 224 (2002).

[20]J. Li, G. Jia, and Z. Lin, Organometallics **27**, 3892 (2008).

[21]C. C. Lu, C. T. Saouma, M. W. Day, and J. C. Peters, J. Am. Chem. Soc. **129**, 4 (2006).

[22]H. I. Karunadasa, E. Montalvo, Y. Sun, M. Majda, J. R. Long, and C. J. Chang, Science **335**, 698 (2012).

[23]B. Hinnemann, P. G. Moses, J. Bonde, K. P. Jørgensen, J. H. Nielsen, S. Horch, I. Chorkendorff, and J. K. Nørskov, J. Am. Chem. Soc. **127**, 5308 (2005).

[24]R. R. Chianelli, M. H. Siadati, M. P. De la Rosa, G. Berhault, J. P. Wilcoxon, R. Bearden, Jr., and B. L. Abram, Catal. Rev. **48**, 1 (2006).

[25]T. F. Jaramillo, K. P. Jørgensen, J. Bonde, J. H. Nielsen, S. Horch, and I. Chorkendorff, Science **317**, 100 (2007).

[26]M. Asadi, B. Kumar, A. Behranginia, B. A. Rosen, A. Baskin, N. Repnin, D. Pisasale, P. Phillips, W. Zhu, R. Haasch, R. F. Klie, P. Krá, J. Abiade, and A. Salehi-Khojin, Nat. Commun. **5**, 1 (2014).

[27]W. Martin, J. Baross, D. Kelley, and M. J. Russell, Nat. Rev. Microbiol. **6**, 805 (2008).

[28]G. D. Cody, Annu. Rev. Earth Planet. Sci. **32**, 569 (2008).

[29]M. J. Russell and A. J. Hall, J. Geol. Soc. **154**, 377 (1997).

[30]G. Wächtershäuser, Prog. Biophys. Mol. Biol. **58**, 85 (1992).

[31]A. Roldan, N. Hollingsworth, A. Roffey, H.-U. Islam, J. B. M. Goodall, C. R. A. Catlow, J. A. Darr, W. Bras, G. Sankar, K. B. Holt, G. Hogarth, and N. H. de Leeuw, Chem. Commun. **51**, 7501 (2015).

[32]S. Haider, A. Roldan, and N. H. de Leeuw, J. Phys. Chem. C **118**, 1958 (2014).

[33]N. Y. Dzade, A. Roldan, and N. H. de Leeuw, J. Chem. Phys. **139**, 124708 (2013).

[34]N. Y. Dzade, A. Roldan, and N. H. de Leeuw, Phys. Chem. Chem. Phys. **16**, 15444 (2014).

[35]A. Parkin, J. Seravalli, K. A. Vincent, S. W. Ragsdale, and F. A. Armstrong, J. Am. Chem. Soc. **129**, 10328 (2007).

[36]H. A. Hansen, J. B. Varley, A. A. Peterson, and J. K. Nørskov, J. Phys. Chem. Lett. **4**, 388 (2013).

[37]C. Huber and G. Wächtershäuser, Science **276**, 245 (1997).

[38]D. Rickard and G. W. Luther, Chem. Rev. **107**, 514 (2007).

[39]G. Kresse and J. Furthmuller, Comput. Mater. Sci. **6**, 15 (1996).

[40]G. Kresse and J. Furthmuller, Phys. Rev. B **54**, 11169 (1996).

[41]G. Kresse and J. Hafner, Phys. Rev. B **48**, 13115 (1993).

[42]G. Kresse and J. Hafner, J. Phys.: Condens. Matter **6**, 8245 (1994).

[43]S. Grimme, J. Comput. Chem. **27**, 1787 (2006).

[44]J. P. Perdew and A. Zunger, Phys. Rev. B **23**, 5048 (1981).

[45]J. P. Perdew, J. A. Chevary, S. H. Vosko, K. A. Jackson, M. R. Pederson, D. J. Singh, and C. Fiolhais, Phys. Rev. B **46**, 6671 (1992).

[46]P. E. Blöchl, Phys. Rev. B **50**, 17953 (1994).

[47]G. Kresse and D. Joubert, Phys. Rev. B **59**, 1758 (1999).

[48]H. J. Monkhorst and J. D. Pack, Phys. Rev. B **13**, 5188 (1976).

[49]A. R. Lennie, S. A. T. Redfern, P. F. Schofield, and D. J. Vaughan, Mineral. Mag. **59**, 677 (1995).

[50]A. R. Lennie, S. A. T. Redfern, P. E. Champness, C. P. Stoddart, P. F. Schofield, and D. J. Vaughan, Am. Mineral. **82**, 302 (1997); available at http://www.minsocam.org/MSA/amMin/toc/Articles_Free/1997/Lennie_p302-309_97.pdf.

[51]R. A. Berner, Science **137**, 669 (1962).

[52]E. F. Bertaut, P. Burlet, and J. Chappert, Solid State Commun. **3**, 335 (1965).

[53]D. J. Vaughan and M. S. Ridout, J. Inorg. Nucl. Chem. **33**, 741 (1971).

[54]A. J. Devey, R. Grau-Crespo, and N. H. de Leeuw, J. Phys. Chem. C **112**, 10960 (2008).

[55]A. Subedi, L. J. Zhang, D. J. Singh, and M. H. Du, Phys. Rev. B **78**, 134514 (2008).

[56]J. Brgoch and G. J. Miller, J. Phys. Chem. A **116**, 2234 (2012).

[57]H. Ohfuji and D. Rickard, Earth Planet. Sci. Lett. **241**, 227 (2006).

[58]G. W. Watson, E. T. Kelsey, N. H. de Leeuw, D. J. Harris, and S. C. Parker, J. Chem. Soc., Faraday Trans. **92**, 433 (1996).

[59]P. W. Tasker, J. Phys. C: Solid State Phys. **12**, 4977 (1979).

[60]G. Henkelman, A. Arnaldsson, and H. Jonsson, Comput. Mater. Sci. **36**, 354 (2006).

[61]R. F. W. Bader, *Atoms in Molecules: A Quantum Theory* (Oxford University Press, London, 1994).

[62]G. Mills, H. Jónsson, and G. K. Schenter, Surf. Sci. **324**, 305 (1995).

[63]A. Ulitsky and R. Elber, J. Chem. Phys. **92**, 1510 (1990).

[64]B. Hammer and J. K. Nørskov, Adv. Catal. **45**, 71 (2000).